Enhancing Oxygen Exchange Activity by Tailoring Perovskite Surfaces

*Yuan Cheng, Abhinav S. Raman, Julian Paige, Liang Zhang, Danyi Sun, Mavis U. Chen, Aleksandra Vojvodic, Raymond J. Gorte, and John M. Vohs**

Department of Chemical and Biomolecular Engineering

University of Pennsylvania, Philadelphia, PA USA

Abstract

A detailed understanding of the effects of surface chemical and geometric composition is essential for understanding the electrochemical performance of the perovskite (ABO_3) oxides commonly used as electrocatalysts in the cathodes of ceramic fuel cells. Herein, we report how the addition of submonolayer quantities of A- and B-site cations affect the rate of the Oxygen Reduction Reaction (ORR) of Sr-doped $LaFeO_3$ (LSF), $LaMnO_3$ (LSM), and $LaCoO_3$ (LSCo). Density functional theory (DFT) calculations were performed to determine the stability of different active sites on a collection of surfaces. With LSF and LSM, rates for ORR are significantly higher on the A-site terminated surface, while surface termination is less important for LSCo. Our findings highlight the importance of tailoring the surface termination of the perovskite to obtain its ultimate ORR performance.

Keywords: Oxygen Reduction Reaction, Electrocatalysis, Cathode, Solid Oxide Fuel Cells

TOC Graphics

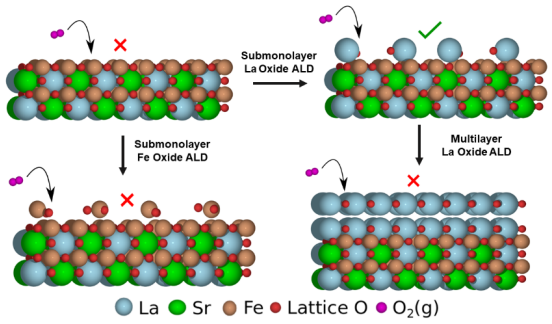

Enhancing oxygen reduction activity by controlling the surface chemistry of the perovskite-structured (ABO_3) mixed oxides used as cathodes in ceramic fuel cells has been a long-term goal for improving stability and performance. The surface composition (chemical and geometric) may not be the same as that of the bulk, and is often not known, due to segregation of the constituent cations during the high-temperature treatments required for cell manufacture[1,2,3]. Therefore, it is generally not clear which surface structures should be targeted. In an effort to provide insight into how surface composition affects performance, several recent studies have used controlled deposition of thin films to modify cathode surfaces[4–6]. Recent studies by Rupp *et al.*[7] and Rahmanipour *et al.*[8] have attempted to elucidate the nature of the active sites on $La_{1-x}Sr_xCoO_{3-\delta}$ (LSCo) and $La_{1-x}Sr_xFeO_{3-\delta}$ (LSF), respectively, by molecular engineering of the surfaces through controlled deposition of the component oxides; however, these studies have generated additional questions. For example, it was reported that the addition of an A-site oxide (SrO) diminishes the performance of LSCo[7], while the addition of La_2O_3 to LSF enhanced performance[8]. In the work reported herein, we used combined experimental and theoretical studies to demonstrate that significant differences exist in the surfaces of LSF, LSCo, and $La_{1-x}Sr_xMnO_{3-\delta}$ (LSM) that help to explain why these materials exhibit significantly different behaviors. Atomic layer deposition (ALD) of A and B site ions was used to provide atomic-level control of surface composition (see Figure 1) of real-world, high-performance cathodes and allowed us to investigate how the terminating sequence of the perovskite affects performance. Observation of significant changes in catalytic properties with changes in the sequence of the terminating atoms on LSF and LSM surfaces, coupled with density functional theory (DFT) calculations of the stability of each surface, was used to determine the optimal surface composition for these perovskites.

Commented [VJM1]: Need to include here all of the references suggested by reviewer 1, and 7,8 below.

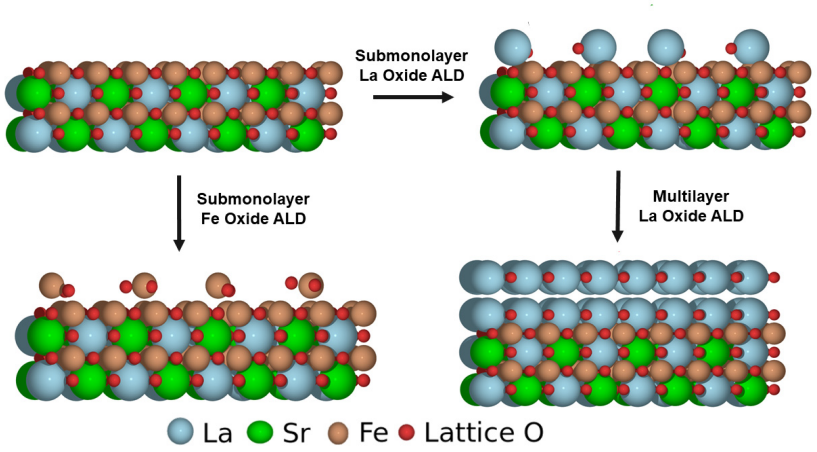

Figure 1. Schematic showing the different ALD-modified surfaces that were investigated in this study.

Electrochemical performance measurements were made using 1 cm diameter symmetric button cells that were prepared from yttria-stabilized-zirconia (YSZ), porous-dense-porous, tri-layer wafers consisting of a dense 80-µm-thick layer sandwiched between two 35-µm-thick, 60%-porous layers with 2-µm pores. 30 wt% LSF, LSM or LSCo was added to the porous layers using infiltration of aqueous salt solutions followed by annealing in air. Details of the cell preparation are in previous publications[9,10,11] and the supplemental information. Decoration of the perovskite surface with submonolayer amounts of A- or B-site cations was achieved using ALD with $Sr(TMHD)_2$, $La(TMHD)_3$, $Pr(TMHD)_3$, $Ca(TMHD)_2$, and $Mn(TMHD)_3$, (TMHD = 2,2,6,6-tetramethyl-3,5-heptanedionato) precursors. Cation deposition rates per ALD cycle (measured gravimetrically using a high surface area alumina support) are given Table S1 and were between

$5 \cdot 10^{13}$ and $8 \cdot 10^{13}$ metal atoms cm^{-2}, corresponding to ≤0.1 monolayer per cycle, for each of the metal oxides.

Low-energy ion scattering (LEIS) provided a measure of the outermost surface chemical composition and was used to confirm the number of ALD cycles required to obtain a monolayer coverage. LEIS studies were performed on a porous LSF-YSZ electrode that was calcined to 1123 K and a dense LSF slab that had been annealed to 1473 K prior to ALD deposition. The LEIS spectrum of the pristine LSF slab, Figure 2a, exhibits the expected peaks for La, Sr, and Fe. The Sr peak is the most intense due to surface enrichment which is known to occur upon high-temperature annealing in air[1,3,12]. Figure 2b shows the LEIS spectrum of this sample after 5 La_2O_3 ALD cycles. Note that this spectrum is now dominated by the La peak. Quantitative analysis of this spectrum indicates that the surface La cation (La_2O_3) coverage is somewhat less than a monolayer (ML), consistent with the ALD growth rate reported in Table S1 which predicts that 5 ALD cycles would produce a La cation coverage of ~0.4 ML (based on the cation density on LSF(100) which is $6.5 \cdot 10^{14}$ cm^{-2}). The LEIS data for the porous LSF-YSZ electrode prior to ALD modification (Figure 2c) shows that Sr segregation did not occur to an appreciable extent for the low-temperature synthesis conditions, resulting in a more stoichiometric LSF surface. Consistent with the LSF slab data and the gravimetrically-measured growth rates, 10 La_2O_3 ALD cycles was sufficient to form a complete monolayer coating of La_2O_3 (Figure 2d).

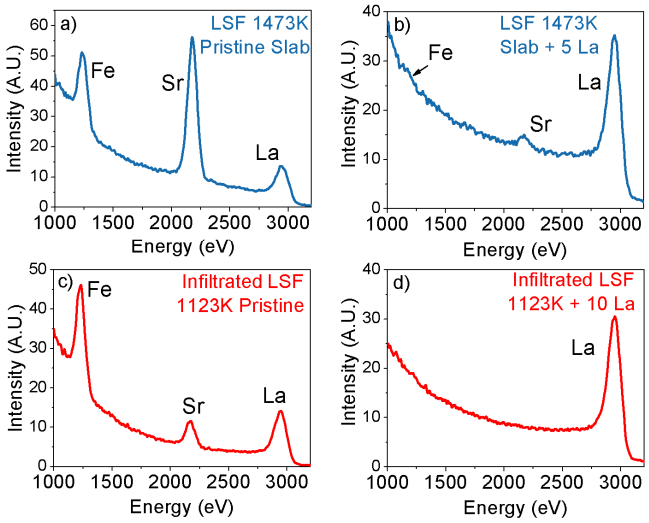

Figure 2. LEIS spectra obtained from (a) a pristine LSF slab that had been sintered at 1473 K, (b) the sample in (a) after 5 La ALD cycles, (c) a pristine high-surface area infiltrated LSF-YSZ composite cathode that had been sintered at1123 K and (d) the sample in (c) after 10 La ALD cycles.

To investigate the effect of decorating the surface of an infiltrated LSF-YSZ electrode with La_2O_3, electrochemical impedance measurements were made for symmetric cells after 5, 10, 20, and 55 La_2O_3 ALD cycles. These samples were oxidized in air at 773 K for 5 min after each ALD cycle, and the impedance spectra were collected with the cell exposed to air at 873 K. These data are displayed in Figure 3a (the ohmic part of each spectrum has been subtracted to facilitate comparison), and the electrode polarization resistance, R_p, extracted from these data are plotted in Figure 3c. After 5 La_2O_3 ALD cycles, corresponding to ~0.5 ML La_2O_3, R_p decreased from that of the pristine cell, 0.48 $\Omega \cdot cm^2$, to 0.27 $\Omega \cdot cm^2$. As shown in Figure S1, this enhancement of electrode

catalytic properties upon surface decoration with sub-monolayer amounts of La_2O_3 was observed for LSF electrodes prepared to have bulk compositions that were both A- and B-site deficient. Enhanced electrode performance was maintained after 10 La_2O_3 ALD cycles which gave an R_p of 0.32 $\Omega \cdot cm^2$. However, additional La_2O_3 increased R_p monotonically. After 55 cycles, corresponding to $2.8 \cdot 10^{15}$ La atoms$\cdot cm^{-2}$, R_p was 0.82 $\Omega \cdot cm^2$ which is more than twice that of the pristine cell.

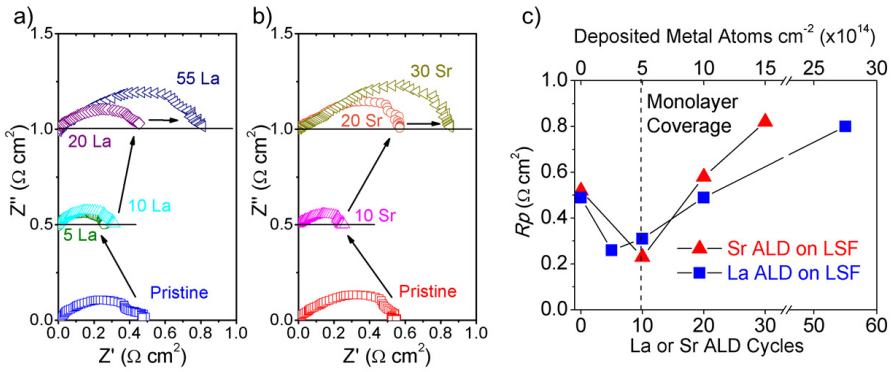

Figure 3. Impedance spectra obtained from infiltrated LSF/YSZ composite cathodes as a function of the number of (a) La ALD cycles and (b) Sr ALD cycles. The polarization resistance, R_p, extracted from the impedance spectra as a function of the number of ALD cycles and number of metal atoms deposited for each sample is plotted in panel (c).

The beneficial effect on catalytic properties and R_p in the sub-monolayer regime was not limited to La_2O_3; and LSF surfaces decorated with other A-site perovskites elements, including Sr, Ca, and Pr, produced a similar effect. Figure 3b displays impedance spectra for an LSF-YSZ cathode as a function of the number of SrO ALD cycles; and, similar to the observations with La_2O_3, R_p was found to decrease from 0.55 $\Omega \cdot cm^2$ to 0.26 $\Omega \cdot cm^2$ after 10 ALD cycles ($\leq$ 1 ML), then

increase with further SrO deposition, reaching 0.85 $\Omega \cdot cm^2$ after 30 SrO ALD cycles. Figure S2 displays the analogous data for LSF cathodes decorated with Pr_2O_3 and CaO and shows the same trends in electrode performance with submonolayer coverages of these oxides. The effect of submonolayer-level surface modification of LSF with A-site cations is summarized in Figure 4 which gives the percentage change in the cathode area-specific resistance after 5 ALD cycles. In all cases, the decrease in R_p following deposition of A-site cations was close to 50% in the submonolayer regime, with R_p increasing once the ML coverage was obtained. It is noteworthy that, although Sr surface segregation is well known to have a deleterious effect on electrode performance[1,7,13,14], submonolayer addition of SrO significantly enhanced performance. (It is also noteworthy that Mutoro et al. applied Sr decoration on thin-film LSC and enhanced its ORR activity by an order of magnitude, attributed largely to catalytically active interface regions between surface Sr-enriched particles and the LSC surface[15]; in our case, however, cannot confirm if the mechanisms are the same) ALD was also used to determine the effect of terminating the LSF surface with the B-site cations, Fe and Mn, and an inert oxide, Zr. Impedance data for Mn deposition is displayed in Figure S3, while data for Fe and Zr were reported elsewhere[5]. Results are summarized in Figure 4 and show that terminating with these oxides decreases the catalytic activity of the electrode and increases R_p, regardless of the oxide coverage.

Formatted: Superscript

Commented [VJM2]: Yuan, why did you add this sentence. Which reviewer comment were you addressing here?

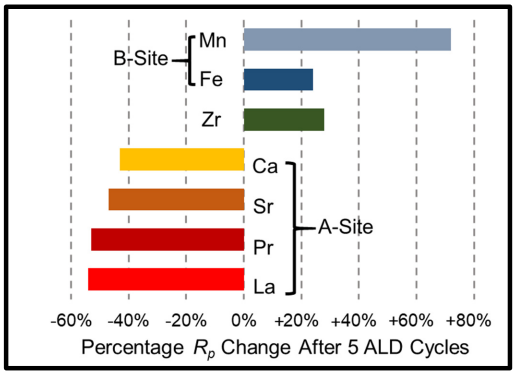

Figure 4. Effect of the addition of submonolayer amounts (5 ALD cycles) of A-site and B-site cations on the R_p of infiltrated LSF/YSZ composite cathodes.

These results further demonstrate that the local atomic structure on the cathode surface plays a pivotal role in determining the catalytic activity for the oxygen reduction and incorporation reactions and thus the overall cathode performance. The fact that submonolayer amounts of La_2O_3 have the same enhancing effect on both stoichiometric and non-stoichiometric LSF cathodes further supports this and shows that, while the bulk composition may affect bulk electron and oxygen ion transport, sites on the surface that are highly active for the oxygen-exchange reaction are needed to obtain high cathode performance.

DFT calculations, which have been successful in modeling the thermodynamic stability as well as ion transport in solid oxide fuel cell (SOFC) materials such as $LaBO_3$[16], LSM[17], LSF[18] and LSCF[19], were performed to determine how surface non-stoichiometry might affect reactivity and whether the various surface terminations explored experimentally are stable. For these simulations, the (001) surface of $LaFeO_3$ was used as a prototypical perovskite surface. Figure 5b shows the calculated stability diagram at 1000 K and P_{O_2} of 0.2 atm for the different $LaFeO_3$ surface

terminations shown in Figure 5a. To determine the stability of the different terminations, we considered their respective surface Gibbs free energies (SGFE) within the region defining the precipitation of bulk La_2O_3 and Fe_2O_3 as a function of the chemical potential of Fe in the system. We found that the stoichiometric BO_2 termination is thermodynamically the most stable surface SOFC operating conditions (yellow vertical region in Figure 5b), indicating that the pristine samples used in the experimental studies were likely to be BO_2 terminated. As shown in Figure 3 and 5c, an improvement in cell performance was observed for systems with sub-monolayer coverages of La_2O_3 deposited using ALD. However, we found that while the stoichiometric AO- and O-terminated AO surfaces are relatively stable, the defective AO surfaces, particularly the ones with AO, A and O vacancies are all thermodynamically unstable under SOFC operating conditions. This is in agreement with the impedance data for an LSF electrode as a function of thermal cycling shown in Figure 5c, where the excellent performance obtained after 10 La_2O_3 ALD cycles goes back to that of pristine LSF upon heating at 973 K for 2 hrs. This suggests that the thermodynamically unstable defective surfaces are likely to be kinetically trapped phases, resulting in their eventual reconstruction to the stable stoichiometric BO_2 surface. It should be noted that preparing the system in one of these metastable, kinetically-trapped states is enabled by the nature of the ALD process, where control can be achieved to the level where the growth results in surfaces with non-uniform surface coverage. We, therefore, hypothesize that, although the surface modification as a result of the sub-monolayer coverage of La_2O_3 does not result in intrinsic thermodynamic stability, the improved cell performance may be attributed to the presence of kinetically-trapped surfaces with AO defects. Going beyond ML coverage of AO units results in reduced cell performance as seen from Figures 3 and 5c. To model this, we considered the stoichiometric AO-terminated surface with an additional A unit consisting of an adatom adsorbed

at the surface. We found that this system is thermodynamically the most unstable among the different surfaces considered under SOFC operating conditions. This suggests that going beyond a ML coverage, should result in a structure with several stoichiometric AO layers, which is thermodynamically more stable, as opposed to those with excess A on the surface. Interestingly, the fact that this is not observed with the thermal cycling, where further ALD modification upon restoration to the pristine cell at 973 K once again improves cell performance, suggests that two different mechanisms may be at play under different conditions.

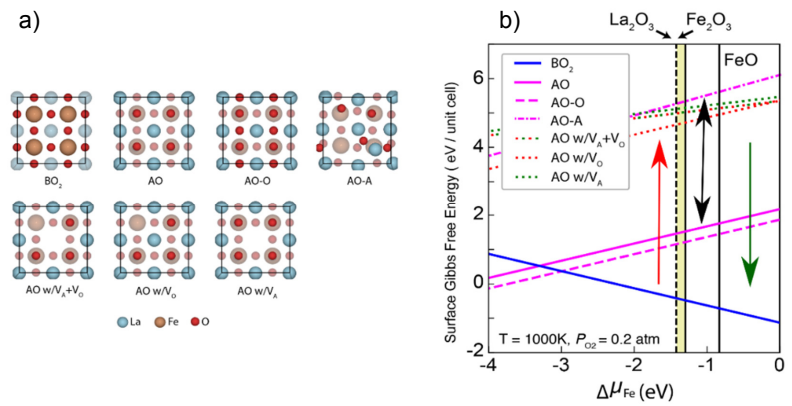

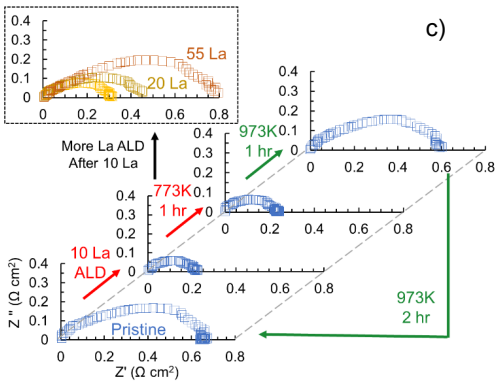

Figure 5. Summary of DFT study of the stability of various terminations of $LaFeO_3$(001). The specific terminations that were studied are shown in (a) and the calculated surface Gibbs free energy for each termination as a function of the Fe chemical potential is plotted in (b), and (c) provides impedance spectra for a composite LSF/YSZ cathode as a function of La ALD cycles and annealing temperature for comparison with the stability calculations.

To examine the generality of the beneficial effect of decorating LSF surfaces with submonolayer quantities of A-site cations, experiments were also performed for symmetric cells with infiltrated LSM-YSZ cathodes infiltrated to 1123 K. (Note: LSM-YSZ electrodes prepared by infiltration and calcined at 1123 K do not exhibit hysteretic behavior upon polarization[20]). Figure 6a shows impedance spectra collected in air at 873 K for one of these cells as a function of the number of La_2O_3 ALD cycles. The trends in these data are similar to those observed for LSF in Figure 3, with R_p decreasing significantly up to monolayer La_2O_3 coverage and then increasing with further La_2O_3 addition. As shown in Figure 6a, the pristine LSM-YSZ electrode had an R_p of 1.4 $\Omega \cdot cm^2$ which decreased to 0.55 and 0.35 $\Omega \cdot cm^2$ after 5 and 10 La_2O_3 ALD cycles, respectively, before gradually

increasing with additional La_2O_3. Impedance data obtained from an LSM-YSZ electrode before and after 5 ALD cycles of SrO, Pr_2O_3, and Mn_2O_3 are shown in Figure S4. These results are again similar to that reported above for LSF with sub-monolayer films of the A-site oxides, SrO and Pr_2O_3, both causing R_p to decrease by ~40%. In contrast, 5 MnO_x ALD cycles had a small effect on R_p (Figure S4c).

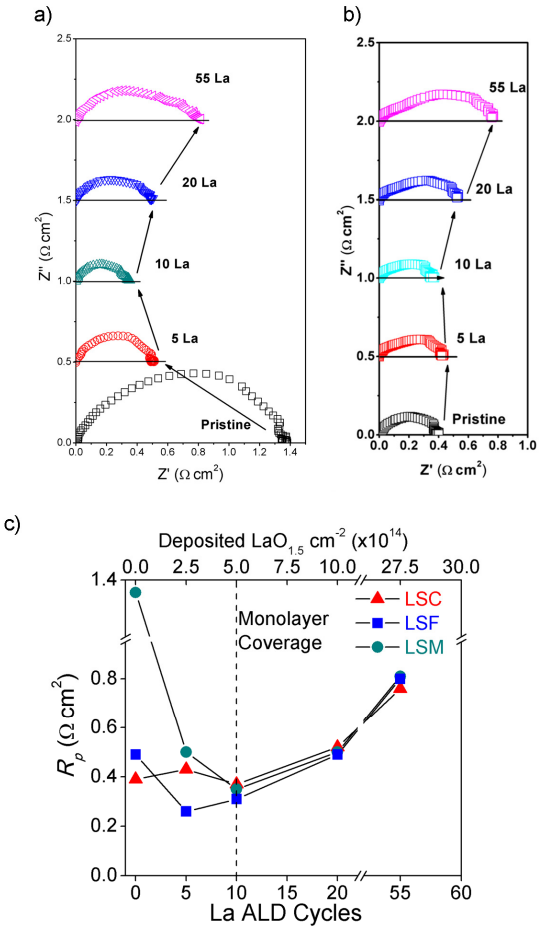

Figure 6. Impedance spectra obtained from (a) infiltrated LSM/YSZ and (b) LSCo/YSZ composite cathodes as a function of the number of La ALD cycles. The polarization resistance, R_p, extracted from the impedance spectra as a function of the number of ALD cycles and number of metal atoms deposited for each sample is plotted in panel (c). To facilitate comparison, data for LSF/YSZ composite electrodes (from Figure 3) is also include in this plot.

The fact that the same performance trends were observed for ALD-modified LSF and LSM surfaces is quite interesting. LSM is known for being a relatively poor cathode due to its lack of ionic conductivity [21,22,23]. However, as shown in a modeling study by Bidrawn *et al.*, cathodes prepared by infiltration into porous YSZ scaffolds do not require high ionic conductivity from the perovskite since the ionic conductivity is provided by the scaffold[24]. These calculations suggested that, for electrodes prepared by infiltration, ionic conductivity of the infiltrated phase does not limit performance as long as the ionic conductivity is above about 10^{-7} S·cm^{-1} (973 K). Therefore, the poor performance of the pristine infiltrated LSM cathode used here is likely due to slow surface kinetics. It was possible to increase oxygen surface exchange so as to decrease the cathode impedance to 0.35 Ω·cm^2 at 873 K. Furthermore, only 5 ALD cycles of the B-site oxide, MnO_x, onto LSF doubled R_p. These data suggest that pristine LSM is also BO_2 (MnO_2) terminated, resulting in sluggish rates for the surface oxygen exchange reaction. Therefore, an AO-terminated surface is also catalytically beneficial for $LaMnO_3$ systems.

Finally, ALD modification of LSCo-YSZ electrodes was also investigated. In this case, enhancement of cathode performance was not observed upon addition of submonolayers of La_2O_3, a result that is consistent with the recent study by Rupp *et al.*[7]. As shown in Figure 6b, the R_p of pristine LSCo was 0.40 Ω·cm^2 and was unaffected by the ALD deposition of up to 1 ML of La_2O_3. Higher La_2O_3 coverages decreased cathode performance, as expected. For LSF and LSM, the

experimental and theoretical results all point to the requirement to have highly-defective, A-site terminated surfaces for achieving high catalytic activity for the surface oxygen exchange reaction. We achieved this using ALD to add submonolayer amounts of the A-site cations to select materials and surfaces. By necessity, such surfaces contain a high concentration of oxygen vacancies which are most likely the active sites for oxygen adsorption. LSCo, however, is much more easily reduced compared to LSM and LSF[25,26,27] The nonstoichiometry (δ) of 40% Sr doped LSCo, LSF and LSM are 0.11 (extrapolated), 0.06 and 0 at 1073K, respectively[25,26,27].~~; and,~~ Therefore, it intrinsically contains a higher concentration of oxygen vacancies and other defects prior to A-site modification. Indeed, this is most likely the reason why LSCo is one of the best cathode materials for SOFC operation at intermediate temperatures[28]; in effect, LSCo already has the optimal surface structure. In the submonolayer regime, the addition of more AO units merely maintains the defect concentration, while multi-layer AO addition ultimately blocks the active sites leading to an increase in R_p.

Commented [VJM3]: Yuan,
I'm not sure what you are trying to say here. Which reviewer comment are you responding to?

In summary, we have demonstrated that ORR rates on perovskite-based SOFC cathodes are strongly affected by the terminating sequence and geometry at the surface. ORR rates are greatly enhanced on LSF and LSM by addition of sub-monolayer quantities of A-site cations, likely because this enhances the surface oxygen vacancy concentration. LSCo is much less sensitive to surface modifications because of its intrinsically higher surface vacancy concentration. These findings call for a better control of the synthesis of the perovskite surfaces at the atomic-scale to obtain SOFC materials with optimal performance.

Associated Content

Supporting Information Available:

1. The experimental methods used for sample preparation and electrochemical measurements.
2. The computational methods used DFT calculations.
3. The ALD growth rate table and the EIS test results mentioned but not presented in the main text.

Author Information

Corresponding author *E-mail vohs@seas.upenn.edu

Acknowledgements

This material is based upon work supported by the Department of Energy under Award Number DE-FE0031252. This report was pre- pared as an account of work sponsored by an agency of the United States Government. Neither the United States Government nor any agency thereof, nor any of their employees, makes any warranty, ex- press or implied, or assumes any legal liability or responsibility for the accuracy, completeness, or usefulness of any information, apparatus, product, or process disclosed, or represents that its use would not infringe privately owned rights. Reference herein to any specific commercial product, process, or service by trade name, trademark, manufacturer, or otherwise does not necessarily constitute or imply its endorsement, recommendation, or favoring by the United States Government or any agency thereof. The views and opinions of authors expressed herein do not necessarily state or reflect those of the United States Government or any agency thereof.

References

(1) Oh, D.; Gostovic, D.; Wachsman, E. D. Mechanism of $La_{0.6}Sr_{0.4}Co_{0.2}Fe_{0.8}O_3$ Cathode Degradation. *J. Mater. Res.* **2012**, *27* (15), 1992–1999.

(2) Orikasa, Y.; Crumlin, E. J.; Sako, S.; Amezawa, K.; Uruga, T.; Biegalski, M. D.; Christen, H. M.; Uchimoto, Y.; Shao-Horn, Y. Surface Strontium Segregation of Solid Oxide Fuel Cell Cathodes Proved by In Situ Depth-Resolved X-Ray Absorption Spectroscopy. *ECS Electrochem. Lett.* **2014**, *3* (4), F23–F26.

(3) Druce, J.; Ishihara, T.; Kilner, J. Surface Composition of Perovskite-Type Materials Studied by Low Energy Ion Scattering (LEIS). *Solid State Ionics* **2014**, *262*, 893–896.

(4) Yu, A. S.; Küngas, R.; Vohs, J. M.; Gorte, R. J. Modification of SOFC Cathodes by Atomic Layer Deposition. *J. Electrochem. Soc.* **2013**, *160* (11), F1225–F1231.

(5) Gong, Y.; Palacio, D.; Song, X.; Patel, R. L.; Liang, X.; Zhao, X.; Goodenough, J. B.; Huang, K. Stabilizing Nanostructured Solid Oxide Fuel Cell Cathode with Atomic Layer Deposition. *Nano Lett.* **2013**, *13* (9), 4340–4345.

(6) Choi, H. J.; Bae, K.; Grieshammer, S.; Han, G. D.; Park, S. W.; Kim, J. W.; Jang, D. Y.; Koo, J.; Son, J. W.; Martin, M.; et al. Surface Tuning of Solid Oxide Fuel Cell Cathode by Atomic Layer Deposition. *Adv. Energy Mater.* **2018**, *8* (33), 1–9.

(7) Rupp, G. M.; Opitz, A. K.; Nenning, A.; Limbeck, A.; Fleig, J. Real-Time Impedance Monitoring of Oxygen Reduction during Surface Modification of Thin Film Cathodes. *Nat. Mater.* **2017**, *16* (6), 640–645.

(8) Rahmanipour, M.; Cheng, Y.; Onn, T. M.; Donazzi, A.; Vohs, J. M.; Gorte, R. J.

Modification of LSF-YSZ Composite Cathodes by Atomic Layer Deposition. *J. Electrochem. Soc.* **2017**, *164* (7), F879–F884.

(9) Cheng, Y.; Yu, A. S.; Li, X.; Oh, T.-S.; Vohs, J. M.; Gorte, R. J. Preparation of SOFC Cathodes by Infiltration into LSF-YSZ Composite Scaffolds. *J. Electrochem. Soc.* **2016**, *163* (2), F54–F58.

(10) Huang, Y.; Vohs, J. M.; Gorte, R. J. SOFC Cathodes Prepared by Infiltration with Various LSM Precursors. *Electrochem. Solid-State Lett.* **2006**, *9* (5), A237.

(11) Boaro, M.; Vohs, J. M.; Gorte, R. J. Synthesis of Highly Porous Yttria-Stabilized Zirconia by Tape-Casting Methods Synthesis of Highly Porous Yttria-Stabilized Zirconia by Tape-Casting Methods. *J. Am. Ceram. Soc.* **2003**, *86* (3), 395–400.

(12) Koo, B.; Kim, K.; Kim, J. K.; Kwon, H.; Han, J. W.; Jung, W. C. Sr Segregation in Perovskite Oxides: Why It Happens and How It Exists. *Joule*. 2018, pp 1476–1499.

(13) Simner, S. P.; Anderson, M. D.; Engelhard, M. H.; Stevenson, J. W. Degradation Mechanisms of La–Sr–Co–Fe–O_3 SOFC Cathodes. *Electrochem. Solid-State Lett.* **2006**, *9* (10), A478.

(14) Chen, Y.; Jung, W.; Cai, Z.; Kim, J. J.; Tuller, H. L.; Yildiz, B. Impact of Sr Segregation on the Electronic Structure and Oxygen Reduction Activity of $SrTi_{1-x}$ Fe_xO_3 Surfaces. *Energy Environ. Sci.* **2012**, *5* (7), 7979–7988.

(15) Mutoro, E.; Crumlin, E. J.; Biegalski, M. D.; Christen, H. M.; Shao-Horn, Y. Enhanced Oxygen Reduction Activity on Surface-Decorated Perovskite Thin Films for Solid Oxide Fuel Cells. *Energy Environ. Sci.* **2011**, *4* (9), 3689–3696.

(16) Lee, Y. L.; Kleis, J.; Rossmeisl, J.; Morgan, D. Ab Initio Energetics of LaBO3(001) (B=Mn, Fe, Co, and Ni) for Solid Oxide Fuel Cell Cathodes. *Phys. Rev. B - Condens. Matter Mater. Phys.* **2009**, *80* (22), 1–20.

(17) Mastrikov, Y. A.; Merkle, R.; Heifets, E.; Kotomin, E. A.; Maier, J. Pathways for Oxygen Incorporation in Mixed Conducting Perovskites: A DFT-Based Mechanistic Analysis for (La, Sr)$MnO_{3-\delta}$. *J. Phys. Chem. C* **2010**, *114* (7), 3017–3027.

(18) Mizusaki, J.; Yoshihiro, M.; Yamauchi, S.; Fueki, K. Nonstoichiometry and Defect Structure of the Perovskite-Type Oxides $La_{1-x}Sr_xFeO_{3-\delta}$. *J. Solid State Chem.* **1985**, *58* (2), 257–266.

(19) Mastrikov, Y. A.; Merkle, R.; Kotomin, E. A.; Kuklja, M. M.; Maier, J. Formation and Migration of Oxygen Vacancies in $La_{1-x}Sr_xCo_{1-y}Fe_yO_{3-\delta}$ perovskites: Insight from Ab Initio Calculations and Comparison with $Ba_{1-x}Sr_xCo_{1-y}Fe_yO_{3-\delta}$. *Phys. Chem. Chem. Phys.* **2013**, *15* (3), 911–918.

(20) Huang, Y.; Vohs, J. M.; Gorte, R. J. Characterization of LSM-YSZ Composites Prepared by Impregnation Methods. *J. Electrochem. Soc.* **2005**, *152* (7), A1347.

(21) Sun, C.; Hui, R.; Roller, J. Cathode Materials for Solid Oxide Fuel Cells: A Review. *J. Solid State Electrochem.* **2010**, *14* (7), 1125–1144.

(22) Jiang, S. P. A Review of Wet Impregnation—An Alternative Method for the Fabrication of High Performance and Nano-Structured Electrodes of Solid Oxide Fuel Cells. *Mater. Sci. Eng. A* **2006**, *418* (1–2), 199–210.

(23) Vohs, J. M.; Gorte, R. J. High-Performance SOFC Cathodes Prepared by Infiltration. *Adv.*

Mater. **2009**, *21* (9), 943–956.

(24) Bidrawn, F.; Küngas, R.; Vohs, J. M.; Gorte, R. J. Modeling Impedance Response of SOFC Cathodes Prepared by Infiltration. *J. Electrochem. Soc.* **2011**, *158* (5), B514.

(25) Søgaard, M.; Vang Hendriksen, P.; Mogensen, M. Oxygen Nonstoichiometry and Transport Properties of Strontium Substituted Lanthanum Ferrite. *J. Solid State Chem.* **2007**, *180* (4), 1489–1503.

(26) J. Mizusaki, Y. Mima, S. Yamauchi, K. Fueki, and H. T. Nonstoichiometry of the Perovskite-Type Oxides $La_{1-x}Sr_xCoO_{3-\delta}$. *J. Solid State. Chem* **1989**, *80*, 102–111.

(27) Mizusaki, J.; Mori, N.; Takai, H.; Yonemura, Y.; Minamiue, H.; Tagawa, H.; Dokiya, M.; Inaba, H.; Naraya, K.; Sasamoto, T.; et al. Oxygen Nonstoichiometry and Defect Equilibrium in the Perovskite-Type Oxides $La_{1-x}Sr_xMnO_{3-\delta}$. **2000**, *129*, 163–177.

(28) Gorte, R. J.; Vohs, J. M. Catalysis in Solid Oxide Fuel Cells. *Annu. Rev. Chem. Biomol. Eng.* **2011**, *2* (1), 9–30.